THE JOURNAL OF PHYSICAL CHEMISTRY C
A JOURNAL OF THE AMERICAN CHEMICAL SOCIETY

pubs.acs.org/JPCC

Article

Beyond Simple Structure–Function Relationships: The Interplay of Geometry, Electronic Structure, and Molecule/Electrode Coupling in Single-Molecule Junctions

Nathan D. Bamberger, Dylan Dyer, Keshaba N. Parida, Tarek H. El-Assaad, Dawson Pursell, Dominic V. McGrath, Manuel Smeu, and Oliver L. A. Monti*

Cite This: J. Phys. Chem. C 2022, 126, 6653–6661

Read Online

ACCESS | Metrics & More | Article Recommendations | Supporting Information

ABSTRACT: Structure–function relationships constitute an important tool to investigate the fundamental principles of molecular electronics. Most commonly, this involves identifying a potentially important molecular structural element, followed by designing and synthesizing a set of related organic molecules, and finally interpretation of their experimental and/or computational quantum transport properties in the light of this structural element. Though this has been extremely powerful in many instances, we demonstrate here the common need for more nuanced relationships even for relatively simple structures, using both experimental and computational results for a series of stilbene derivatives as a case study. In particular, we show that the presence of multiple competing and subtle structural factors can combine in unexpected ways to control quantum transport in these molecules. Our results clarify the reasons for previous widely varying and often contradictory reports on charge transport in stilbene derivatives and highlight the need for refined multidimensional structure–property relationships in single-molecule electronics.

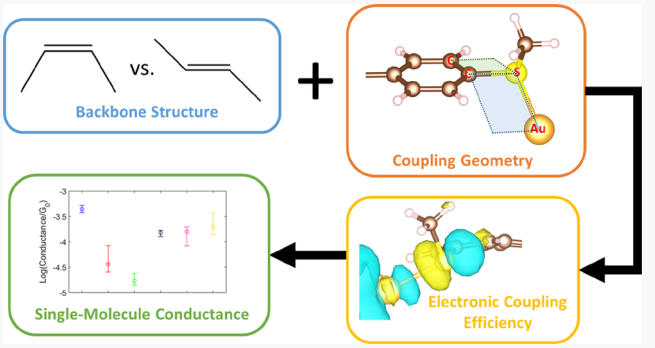

1. INTRODUCTION

The field of molecular electronics—which involves building circuits incorporating individual small organic molecules as components[1]—has the potential to enable smaller, more efficient, and more flexible electronic devices in the future[2] and also serves as a useful testbed for fundamental investigations of quantum transport and molecular physical chemistry.[3] To advance both of these goals, predictive structure–property relationships are needed that allow transport properties to be intentionally controlled via molecular design. This widely embraced goal in the molecular electronics research community usually proceeds by identifying a potentially important design element in a molecular structure, followed by testing this prediction with a series of structurally related molecules that seemingly isolate the importance of this particular element.[4−8] While this often constitutes a powerful approach, it ignores the potential for interaction—deliberate or undesired—between multiple coupled degrees of freedom for molecules in a junction. As a consequence, seemingly minor modifications to the molecular structure may result in widely different transport behavior, confounding the interpretation in terms of underlying principles.

One such case where this is quite evident is cis vs trans isomers of stilbene-like moieties,[9−13] a structural element that commonly appears in molecular scaffolds considered for electronics applications, especially in the context of photoactivated switches.[14,15] Single-molecule conductance—the most fundamental transport property—has been investigated both theoretically and experimentally for a stilbene-like molecule,[16] as well as for several derivatives of the structurally similar azobenzene moiety.[17−22] However, such studies have produced results varying from an ∼2× higher conductance for cis over trans,[16] to the exact opposite,[21] and even all the way up to ∼100× higher conductance for trans[18] or ∼30× higher conductance for cis.[22] Aside from differences in measurement methodology and slight variations in molecular design, an important reason for this inconsistency is likely that changing from trans to cis unavoidably causes multiple structural changes at once, each of which can affect conductance (Figure 1): the length of the molecule decreases, which is expected to increase conductance by reducing the tunneling barrier width;[23] steric hindrance causes each ring in the cis molecule

Received: February 4, 2022
Revised: March 24, 2022
Published: April 11, 2022

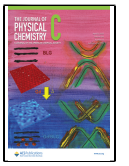

https://doi.org/10.1021/acs.jpcc.2c00761
J. Phys. Chem. C 2022, 126, 6653−6661

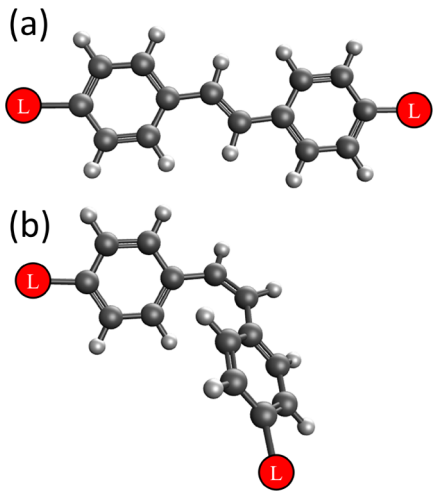

Figure 1. Generic structures of trans (a) and cis (b) stilbene derivatives with para-connected linker groups (represented by red circles), illustrating three key differences that arise upon isomerization: (1) the linker-to-linker length decreases by ∼25%; (2) the second ring twists out of plane with respect to the first; and (3) the two linkers are no longer pointed 180° opposite each other.

to twist out of plane by ∼35°, which is expected to decrease conductance by partially breaking the conjugated π-system;[24−26] the electronic structure of cis and trans isomers and their respective energy-level alignments with the electrodes may differ; and the modified geometry of the molecule, especially the angles at which linkers attached in the standard para positions extend out from the backbone, may impact the orbital alignment between metal and molecule and hence the efficiency of electronic coupling between the two. Attaching linkers in positions other than para often produces destructive quantum interference,[27] which would add yet another confounding factor influencing conductance. Therefore, while most previously developed structure−property relationships focus on one design property at a time,[6,24,28−30] the effects of cis/trans isomerization on single-molecule conductance cannot be expected to be as simple. Instead, a more nuanced structure−property relationship is required that considers the roles of multiple effects simultaneously, especially interactions between them.

In particular, previous results have suggested that differences in how cis and trans geometries influence molecule/metal coupling may play an important role in determining single-molecule conductance. For example, calculations by Osella et al.[19] suggested that chemisorption vs physisorption produce opposite cis/trans conductance orderings, and Martin et al.[16] rationalized their experimental results by positing that the cis geometry leads to stronger coupling by allowing not just the linker groups but also one phenyl ring to come into close contact with the metal electrode. Nevertheless, these effects remain poorly understood. One especially important case that has not yet been explored is how the coupling of conformationally flexible linker groups to the metal electrodes might be differentially affected by cis vs trans backbone geometries. This possibility is motivated by density functional theory (DFT) calculations for the common −SMe (methylsulfide) linker group, which have shown that the barrier to rotation of this linker is quite small,[31,32] while at the same time molecule/metal electronic coupling, and hence conductance, is strongly controlled by the angle between the S−Au bond and the π-system, with maximal coupling occurring for a 90° angle.[31,33] Any differences in the geometric constraints that cis and trans geometries place on −SMe linker orientation therefore have the potential to be a major factor by which cis/trans isomerization impacts single-molecule conductance, and such interactions likely apply more generally to other flexible linkers as well.

To investigate this possibility and explore the interactions between cis/trans isomerization and molecular conductance more generally, in this work, we use a combination of experiment and theory to investigate the single-molecule conductance of a series of custom-designed stilbene derivatives functionalized with −SMe linkers (Scheme 1). This series

Scheme 1. Structures and Color/Naming Conventions of the Six OPV2 Molecules Considered in This Work

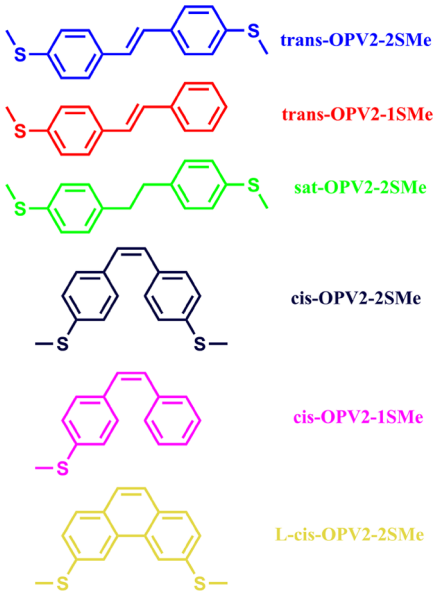

includes the cis and trans versions of this structure (*trans*-OPV2-2SMe and *cis*-OPV2-2SMe), as well as single-linker versions (*trans*-OPV2-1SMe and *cis*-OPV2-1SMe) to help understand the role of −SMe/metal orbital coupling. To help elucidate and control for potential confounding effects from molecular twisting that both breaks the π-system conjugation and potentially forces new linker/electrode geometries, we also include a version of the cis molecule with the rings locked into a fully planar geometry (L-*cis*-OPV2-2SMe) and a version of the molecule with the π-conjugation fully broken by saturating the double-bond linkage (*sat*-OPV2-2SMe). Together, this series thus explores and helps disentangle multiple key design parameters used throughout the single-molecule literature and sheds light on interactions between them that determine molecular conductance. Our study therefore helps clarify the reasons for the widely differing reported conductance values for seemingly similar molecular structures with cis vs trans double bonds.

In the remainder of this paper, we present experimental evidence that, in doubly anchored stilbene derivatives, the geometric constraints of the cis geometry result in less efficient metal/molecule electronic coupling, and hence lower conductance, compared to the trans geometry. We also show how this interaction between backbone conformation and linker orientation can explain the striking observation that *cis*-OPV2-

https://doi.org/10.1021/acs.jpcc.2c00761
J. Phys. Chem. C 2022, 126, 6653−6661

2SMe, *cis*-OPV2-1SMe, and L-*cis*-OPV2-2SMe all display essentially the same peak conductance value. We then use computational results to support these interpretations and offer additional insight into how the −SMe linker orientation affects single-molecule conductance. These findings illustrate the limitations of "divide-and-conquer" structure−function relationships in systems where multiple effects interact, and the need to begin to develop more nuanced relationships that will help the readily accessible cis/trans structural motif to be predictively used to control conductance. In addition, these results highlight the fact that the potential complexity introduced by −SMe linkers—and likely other common linkers with conformational flexibility as well—must be taken into account when designing molecules for transport experiments.

2. METHODS

2.1. Experimental Methods. The experimental conductance of each OPV2 molecule from Scheme 1 was measured using a custom-built mechanically controlled break junction (MCBJ) setup described previously.[4,34,35] Briefly, MCBJ samples were fabricated on a phosphor bronze substrate coated with an insulating layer of polyimide. A pattern containing a thin (∼100 nm) gold constriction was defined with electron beam lithography and then coated with 4 nm of titanium and 80 nm of gold. Reactive ion etching with an O_2/CHF_3 plasma was used to underetch the polyimide and create an ∼1 μm long free-standing gold bridge.

To collect breaking traces, each sample was clamped into a custom three-point bending apparatus with a push rod controlled by both a stepper motor (for coarse movements) and a 40 μm piezo actuator (for movement during trace collection). Conductance through the gold bridge or nanogap was measured at 20 kHz while applying a 100 mV bias, using a custom high-bandwidth Wheatstone bridge amplifier.[36] For each trace, coarse movements were used to achieve a junction conductance between 5 and 7 G_0 (1 G_0 = 77.48 μS,[37] the quantum of conductance), and then the piezo was extended at 60 μm/s to break the bridge while recording trace data. Thousands of traces were collected for each sample using a custom LabVIEW program.

All molecules were synthesized on site and characterized by NMR and mass spectrometry (Supporting Information Section S.1). Molecular solutions of 1 and/or 10 μM concentration in HPLC grade (>99.7%, Alfa Aesar) dichloromethane (DCM) were created for deposition on MCBJ samples. For each sample, 2000+ consecutive breaking traces were collected after the deposition of pure DCM as a negative control and to determine a junction attenuation ratio.[34] Next, the molecular solution was deposited inside a Kalrez gasket placed in the center of the sample using a clean glass syringe. Following the approach of Bamberger et al.,[34] multiple data sets were collected using each sample, and data sets from at least two distinct samples were collected for each molecule (see Supporting Information Section S.2 for details on all data sets used in this work).

The molecular features observed for the OPV2 series often have complex shapes due to convolution with the tunneling background signal, which additionally is known to vary between data sets.[34,38] A segment clustering tool described previously[34] was thus used to unambiguously identify a "main plateau cluster" from each analyzed data set. The conductance distribution of trace segments assigned to each plateau cluster was then fit with a single unrestricted Gaussian to determine a peak conductance value. Following the method of Bamberger et al.,[34] each data set was clustered 12 different times to account for uncertainty in the optimal value of the minPts clustering parameter (see Supporting Information Section S.3 for details).

2.2. Computational Methods. The molecules of interest were first relaxed as isolated species with the Orca code[39] using the B3LYP[40,41] functional with the 6−311++G(d,p) basis set. The relaxed molecules were then placed between Au electrodes that taper to a single Au atom, which interacts directly with the lone pair of the −SMe group (see Figure S16a). For the single-linker versions, the Au atom was arranged to interact directly with the π-system of the benzene ring without the −SMe group (see Figure S16b).

A series of structural relaxations were carried out in the Vienna ab initio simulation package (VASP)[42,43] for each molecule to determine the lowest-energy electrode−electrode separation. We employed the Perdew−Burke−Ernzerhof (PBE)[44] functional with the DFT-D3 method of Grimme[45] to account for van der Waals interactions. The plane-wave cutoff was set to 400 eV, and relaxations continued until residual forces on atoms allowed to relax were lower than 0.02 eV/Å. The optimized molecular junction was then built into a two-probe geometry by extending the Au electrodes (see Figure S16c).

Electron transport was calculated through the optimized two-probe geometries using the nonequilibrium Green's function technique combined with density functional theory (NEGF-DFT), as implemented in the Nanodcal code.[46,47] The NEGF-DFT approach uses the retarded Green's function to obtain the transmission function, $T(E)$, which represents the probability that an electron with a given energy E is transmitted from the left electrode through the molecule into the right electrode. Integrating the transmission function over a specific energy range gives the current for the corresponding bias window. In the limit of the bias voltage approaching zero, the transmission at the Fermi energy gives the low-bias conductance in units of G_0. Details of this approach have been provided in our previous publications.[4,48]

3. RESULTS AND DISCUSSION

3.1. Experimental Results. Representative one-dimensional (1D) conductance histograms for each OPV2 molecule, as well as for pure DCM, are overlaid in Figure 2a. Each of these histograms shows a broad peak whose location is largely reproducible across the other data sets collected with the same molecule (see Supporting Information Section S.3 for further details). Moreover, the main plateau features identified in each data set by segment clustering tend to agree well with these peaks, indicating that segment clustering is reliably extracting molecular signatures (Supporting Information Section S.4), similar to previous results in which this agreement between raw and cluster-specific histograms is discussed in detail.[34] The segment clustering results are summarized in Figure 2b: each point represents the median from among the set of all 12 peak conductance values produced by segment clustering from all data sets collected with each molecule, and the error bars represent the range of the middle 67% of those values.[4] These error bars are thus a measure of the uncertainty due to both data set-to-data set variation and ambiguity about the exact cluster bounds but should not be interpreted as a single universal measure of experimental error.

https://doi.org/10.1021/acs.jpcc.2c00761
J. Phys. Chem. C 2022, 126, 6653−6661

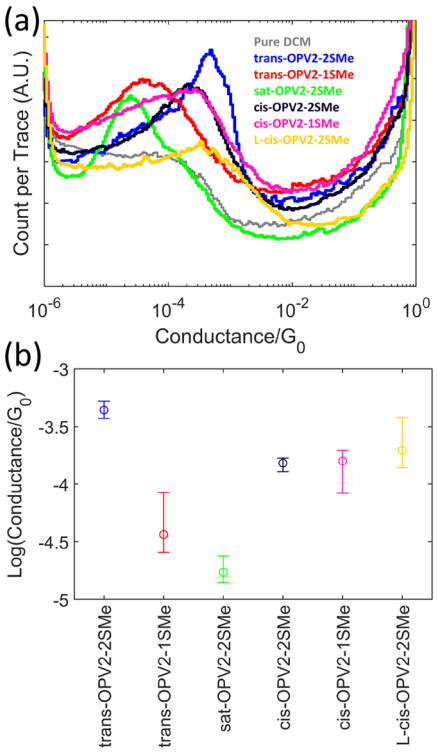

Figure 2. (a) Overlaid example 1D conductance histograms for each OPV2 molecule and a negative control with only DCM, constructed using 2500−10,000 consecutively collected traces (see Supporting Information Section S.2). (b) Summary of the peak conductance values determined for each molecule, across multiple data sets, using Gaussian fits applied to the main plateau clusters identified by segment clustering.

Many of the relative conductance relationships in Figure 2b are in agreement with the predictions of "standard" single-dimensional structure−property rules. For example, going from *trans*-OPV2-2SMe to *sat*-OPV2-2SMe, which fully breaks the conjugated π-system while leaving the molecular length largely unchanged, causes the conductance to drop by over an order of magnitude, which is consistent with both previous measurements[10] and the widely accepted principle that conjugated π-systems extending from linker to linker are needed to produce highly conducting molecules.[5,49] Similarly, multiple studies[13,50−52] have found that single-linker molecules (including *trans*-OPV2 with single −SMe linkers)[13] conduct significantly less than double-linker molecules, and this agrees with our results for *trans*-OPV2-1SMe vs *trans*-OPV2-2SMe. Either direct gold−π coupling[13,50] and/or two-molecule junctions involving π−π stacking[50,52] have been proposed to explain the lower conductance of single-linker molecules, and both structures could arise in our experiments. The apparent lengths of our molecular features suggest, however, that direct gold−π coupling is the more likely explanation (Supporting Information Section S.5).

Strikingly, Figure 2b also reveals the surprising result that approximately the same conductance was measured for all three cis molecules, with all three less conductive than *trans*-OPV2-2SMe. This finding does not conform to "standard" structure−property rules: these might expect the shorter cis molecules to conduct more than the trans; they would further predict *cis*-OPV2-1SMe to have significantly lower conductance than *cis*-OPV2-2SMe, in analogy to the trans structures, and they would predict L-*cis*-OPV2-2SMe to have a conductance perhaps as high or higher than *trans*-OPV2-2SMe due to full conjugation combined with a shorter length. A new, more nuanced structure−property relationship is thus required to explain these results. In particular, the fact that the −2SMe and −1SMe molecules have very different conductances in a trans geometry but similar conductances in a cis geometry suggests that the role of the identical −SMe linker groups must depend on the backbone geometry in some way. We thus next examine the role of those linkers in detail and uncover how they can explain the surprising conductances of each of the three cis molecules.

It has been previously shown by DFT that, for conjugated molecules with −SMe linkers, the orientation of the Au−S bond relative to the π-system—quantified by the Au−S−C−C dihedral angle shown in Figure 3—strongly controls the

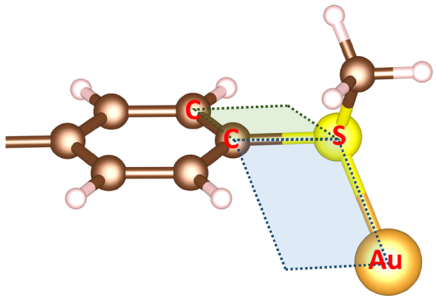

Figure 3. Definition of the Au−S−C−C dihedral angle relevant for molecule−electrode coupling.

strength of metal/molecule electronic coupling and hence conductance. Coupling is maximized at an angle of 90°, which allows the sulfur lone pair involved in the Au−S bond to align with the extended π-system of the molecule, and is minimized at 0°.[31,33] In light of this, we hypothesize that the geometric constraints imposed by the *cis*-OPV2 backbone force the Au−S−C−C angles to spend more time farther from 90°, while in the less-constrained *trans*-OPV2 geometry, these angles are free to spend more time closer to the optimal 90°. As a result, the average metal/molecule electronic coupling in *cis*-OPV2-2SMe and L-*cis*-OPV2-2SMe would be weaker than in *trans*-OPV2-2SMe, explaining the lower conductances we measured for these cis molecules despite their shorter length.

The fact that, relative to *trans*-OPV2-2SMe, conductance is lowered to a similar extent in both *cis*-OPV2-2SMe and L-*cis*-OPV2-2SMe, despite the absence of inter-ring twisting in the locked version, suggests that the weaker metal/molecule electronic coupling caused by the cis geometry is the more important effect in this series of structures. That is not to say that inter-ring twisting has no effect on conductance: the central estimate of conductance for L-*cis*-OPV2-2SMe in Figure 2b is ∼1.3× higher than for *cis*-OPV2-2SMe, on the same order as the factor of ∼2 predicted by the well-known "$\cos^2$ rule" for twisting in conjugated systems[24−26] (though the difference in Figure 2b is small compared to the uncertainties in each measurement). However, even with this modest increase in conductance for the planar locked molecule, L-*cis*-OPV2-2SMe remains about two times less conductive than the longer *trans*-OPV2-2SMe. We thus conclude that weaker metal/linker electronic coupling is the dominant way in which the cis geometry influences conductance in these structures.

https://doi.org/10.1021/acs.jpcc.2c00761
J. Phys. Chem. C 2022, 126, 6653−6661

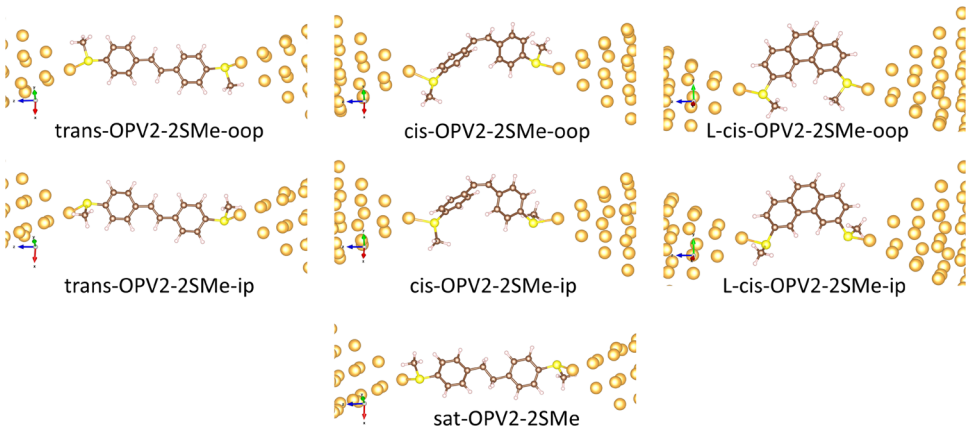

Figure 4. Relaxed structures of each two-linker OPV2 molecule used for NEGF-DFT transport calculations. For *trans*-OPV2-2SMe, *cis*-OPV2-2SMe, and L-*cis*-OPV2-2SMe, two relaxed conformations were generated by starting both S−Au bonds either in-plane (ip) or out-of-plane (oop) with respect to their attached rings and then minimizing the energy. For *sat*-OPV2-2SMe, only a single conformation was considered because saturating the double bond has a much larger effect on conductance than linker orientation.

Finally, to explain the near-identical conductances of *cis*-OPV2-2SMe and *cis*-OPV2-1SMe, we propose that the overall metal/molecule coupling is quite similar between the two molecules, which could occur in two different ways. One possibility is that constrained −SMe/Au binding and direct π/Au binding have similar electronic coupling strengths, and thus the two molecules support similar conductance. Another possibility is that, in *cis*-OPV2-1SMe, the lack of a second point for covalent, mechanical coupling between molecule and electrodes may result in less geometric constraint on the remaining Au−S−C−C angle. In this case, *cis*-OPV2-2SMe would have medium-to-weak, constrained −SMe/Au coupling on both sides, whereas *cis*-OPV2-1SMe would have strong, unconstrained −SMe/Au coupling on one side but weak π/Au coupling on the other, averaging out to produce similar conductance values. In both scenarios, however, it is the effect of geometric constraint on the efficiency of −SMe/Au coupling that plays the key role.

Previous studies considering the role of −SMe linker orientation on single-molecule conductance have focused on how the range of orientations that might be probed by experiment can help explain the breadth of measured conductance distributions or the overall conductance relative to other linker types.[31−33,53,54] The results in this work thus constitute the first experimental evidence that −SMe linker orientation interacts with other structural attributes such as cis vs trans backbone geometry. This type of interaction is an important consideration when using −SMe or other linkers with multiple conformational degrees of freedom and demonstrates that more nuanced structure−property relationships are needed in such cases where multiple structural effects are in play at the same time.

3.2. Computational Results. To further explore the interaction between cis/trans geometry and −SMe/Au coupling efficiency, we carried out NEGF-DFT calculations for the four two-linker OPV2 molecules from Scheme 1. In the case of the two single-linker molecules, calculations may not be able to offer the same level of reliable insights into transport through these structures because of the much larger conformational space available to single-linker molecules, combined with significant ambiguity about how such molecules bind in experimental junctions (see Supporting Information Section S.7 for further details on these sources of ambiguity). In the following discussion, we thus focus exclusively on the computational results for the two-linker molecular structures.

To approximately span the conformational space available to their −SMe linkers, for each of *trans*-OPV2-2SMe, *cis*-OPV2-2SMe, and L-*cis*-OPV2-2SMe, we rotated the methyl groups to create two different junction conformations with both gold−sulfur bonds either primarily in-plane (ip) or out-of-plane (oop) with respect to the phenyl rings and then allowing the geometry to fully relax from each of those starting points. These two relaxed conformations, which we label ip and oop, thus help us consider the two extremes of high- or low-coupling efficiency for each molecule in physically reasonable geometries (Figure 4). This is necessarily an incomplete description of the experimentally probed junctions, which likely sample a large number of conformations (see, e.g., Supporting Information Section S.8), and in which variations in the atomic structure of the electrodes may also affect the −SMe orientations. Nevertheless, these conformations roughly span the available space and aid in interpreting our experimental results. Note that quantitative agreement between NEGF-DFT and experimental results is not expected in any case due to, among other things, the well-known tendency of DFT to underestimate band gaps.[55,56] For *sat*-OPV2-2SMe, only a single conformation is considered since the saturated backbone, rather than linker orientation, dominates molecular conductance.

As shown in Table 1, the Au−S−S−C dihedral angles in both cis molecules are significantly farther from the optimal coupling angle of 90° compared to *trans*-OPV2-2SMe in either the ip or oop conformations. This is consistent with our hypothesis, based on the experimental results, that a cis

Table 1. Au−S−C−C Dihedral Angles D_1 and D_2 and Their Sine-Squared Product for the Relaxed Structures in Figure 4

molecule	D_1 (deg)	D_2 (deg)	$\sin^2(D_1)\sin^2(D_2)$
trans-OPV2-2SMe-oop	97.1	102.3	0.94
cis-OPV2-2SMe-oop	72.5	63.9	0.73
L-*cis*-OPV2-2SMe-oop	60.1	51.9	0.47
trans-OPV2-2SMe-ip	65.0	62.1	0.64
cis-OPV2-2SMe-ip	45.1	38.1	0.19
L-*cis*-OPV2-2SMe-ip	47.1	38.5	0.21

https://doi.org/10.1021/acs.jpcc.2c00761
J. Phys. Chem. C 2022, 126, 6653−6661

backbone imposes geometric constraints that force the −SMe linkers to spend more time in positions that experience weaker metal/molecule electronic coupling. The effect of these deviations on molecular conductance can be approximated by multiplying the square of the sine of each dihedral angle (maximal for $D_1 = D_2 = 90°$), in analogy to how cosine-squared terms are used to approximate the conductance reduction caused by twisting within a π-system.[24−26] As seen in Table 1, this approximation shows that the differences observed in Figure 4 have a significant impact on conductance. It also agrees with the experimental result of higher conductance for the trans- version of the doubly anchored molecule than the two cis- versions.

The transmission functions for each of the conformations in Figure 4 are shown in Figure 5. The Fermi energy (E_F) in these calculations falls very close to the lowest unoccupied molecular orbital (LUMO)-like transmission peak, but NEGF-DFT often misplaces E_F within the highest occupied molecular orbital (HOMO)−LUMO gap,[30,57] and the orbital composition of the −SMe linker is expected to induce HOMO-dominated transport.[5] We therefore focus on the region containing the transmission function minima and the trailing edge of the HOMO peaks (−0.75 to −1.5 eV in the calculated transmission functions; shaded region in Figure 5) to compare the computational results to our low-bias experimental conductance measurements. The ordering of the calculated transmission functions throughout this region is consistent with our experimental measurements. This agreement supports the importance of the limiting computational conformations considered here for understanding transport in these −SMe-linked molecules, and we conclude that the Au−S−C−C angle differences seen in Table 1 are relevant for the systems at hand.

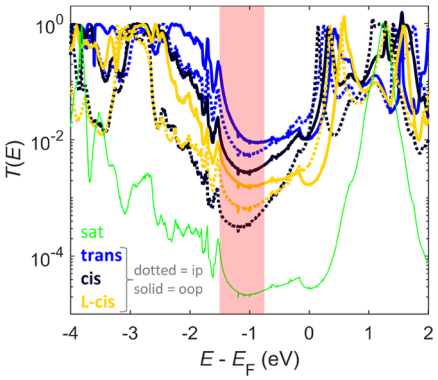

Figure 5. Overlaid transmission functions calculated for each of the conformations shown in Figure 4. For the *trans*, *cis*, and L-*cis* molecules, transmission in the oop and ip orientations is shown in solid and dotted lines, respectively. The red rectangle indicates the expected region of the experimental Fermi energy, E_F (i.e., off-resonant but nearer the HOMO peak than the LUMO peak). The ordering of transmission functions within this region matches the experimentally measured conductances in Figure 2b.

We note that the calculated zero-bias transmission function of *trans*-OPV2-2SMe-ip is larger than that of *cis*-OPV2-2SMe-oop, despite the fact that the Au−S−C−C dihedrals are closer to 90° in the latter. This implies that while the linker orientation may be a large reason for the lower conductance of the cis molecules vis-à-vis *trans*-OPV2-2SMe, additional factors are also at play. We propose that the partially broken conjugation caused by ring twisting in *cis*-OPV2-2SMe, discussed above, explains this extra reduction in conductance. While L-*cis*-OPV2-2SMe overcomes this internal twisting problem, this may be counteracted by the locked-cis backbone keeping the Au−S−C−C angles even farther from the optimal value of 90° than in the unlocked cis structure (see Table 1). In addition, both the transmission functions in Figure 5 and gas-phase ionization energy calculations (SI Section S.9) indicate that L-*cis*-OPV2-2SMe has a slightly larger transport gap than *cis*-OPV2-2SMe, which also partially counteracts the increase in conductance when untwisted. This provides another example of how complete structure−function relationships in single-molecule quantum transport may require the inclusion of multiple competing factors, a central finding of this work.

To probe the impact of -SMe linker orientation on molecular conductance more systematically, we also performed NEGF-DFT calculations on a series of structures with both Au−S-C−C dihedral angles locked at values ranging from 0° to 90°. Rotation of these dihedrals can also be achieved in a more physically plausible way by varying the junction gap size, yielding qualitatively similar results (Supporting Information Section S.10). We used the L-*cis*-OPV2-2SMe structure for this investigation to eliminate the confounding factor of ring-

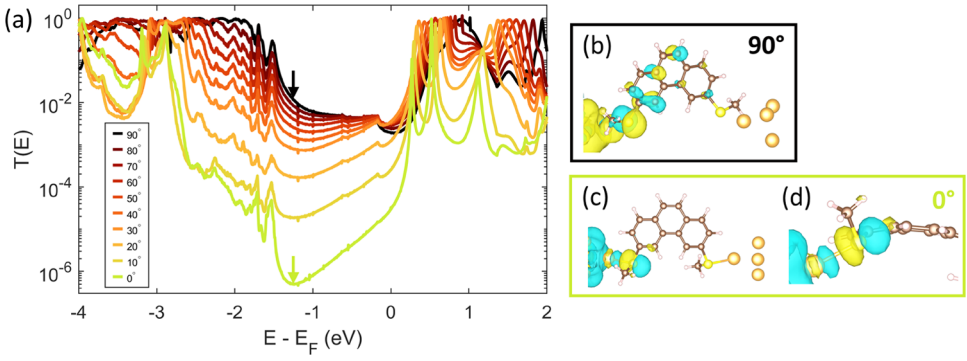

Figure 6. (a) Overlaid transmission functions calculated for L-*cis*-OPV2-2SMe with both Au−S−C−C dihedral angles locked at values ranging from 0 to 90°, demonstrating the pronounced effect this rotation has on molecular conductance. (b) Scattering state for the 90° transmission function from panel (a), calculated at $E - E_F = -1.25$ eV (the dark red arrow in panel (a)). (c, d) Two different views of the scattering state for the 0° transmission function from panel (a), calculated at $E - E_F = -1.25$ eV (the yellow arrow in panel (a)). In particular, the view in panel (d) shows how the wave function on the sulfur is misaligned with the π-system of the molecule, leading to poor electronic coupling efficiency and contributing to the suppressed transmission.

https://doi.org/10.1021/acs.jpcc.2c00761
J. Phys. Chem. C 2022, 126, 6653−6661

twisting degrees of freedom. The most striking feature of the transmission functions for this series of structures (Figure 6a) is that the valley between the HOMO- and LUMO-like transmission peaks becomes much deeper as both Au−S−C−C angles are rotated from 90 to 0°. Examining the scattering states in the window where experimental transport is expected to occur reveals that in the 90° structure (Figure 6b), the electronic wave function is significantly delocalized onto the entire molecule, whereas in the 0° structure (Figure 6c), the wave function does not extend appreciably onto the molecular backbone due to the fact that the orbital symmetry around the sulfur is near-perpendicular to the molecular π-system (Figure 6d). The transmission functions in Figure 6a thus provide direct evidence that the Au−S−C−C dihedral angles are important for controlling metal/molecule electronic coupling efficiency in OPV2-2SMe, in agreement with both the arguments made above and previous findings for conjugated molecules with −SMe linker groups.[31,33]

The transmission functions in Figure 6a reveal that rotating the Au−S−C−C dihedral angles from 90 to 0° also has the effect of shifting the HOMO- and LUMO-like transmission peaks toward more negative energies. As shown in Supporting Information Section S.11, qualitatively similar shifts occur for the molecular transport levels of these same structures in the gas phase, suggesting that this energy-level alignment effect is primarily caused by changes to the molecular structure on its own rather than changes to metal/molecule interactions. In particular, we find that changing the Au−S−C−C dihedral angle also changes the angle between the −SMe and its attached ring, which, in turn, controls how much the sulfur acts as an electron donor to the π-system. The fact that −SMe groups can act as molecular substituents in addition to their role as linker groups thus adds another layer of complexity that must be considered when employing −SMe and similar linkers for use in single-molecule transport applications.

By providing insight into how −SMe linker orientation affects both metal/molecule electronic coupling and energy-level alignment, the full set of transmission functions in Figure 6a thus significantly expands on previous studies, which connected −SMe orientation and conductance using simplified models[31] or only presented transmission functions for one or two −SMe orientations.[33,53]

4. CONCLUSIONS

In summary, we show both experimentally and computationally the multifaceted reasons whereby single-molecule conductance is modified by the simple modification from cis- to trans geometry in −SMe-linked stilbene derivatives. In particular, we find that a dominant role is played by the different ways in which cis and trans geometries constrain the binding conformations available to the −SMe linker groups, which, in turn, control the metal/molecule electronic coupling efficiency and even in-junction molecular electronic structure. Our study thus shows how two common structural attributes and design elements for single-molecule electronics—cis vs trans isomerization and coupling efficiency of flexible linkers such as −SMe—can interact with each other in nontrivial ways to control molecular conductance. These lessons are relevant to single-molecule transport studies employing structural elements in molecular design that induce large geometric changes and to those that rely on conformationally flexible linkers like −SMe as design elements. More generally, this reveals that, in many practical cases, "simple" single parameter structure−property rules and relationships may be insufficient, and instead, more nuanced rules that take such interactions between effects into account are needed.

■ ASSOCIATED CONTENT

Supporting Information

The Supporting Information is available free of charge at https://pubs.acs.org/doi/10.1021/acs.jpcc.2c00761.

Molecular synthesis and characterization; data sets used; comment on *cis*-OPV2-1SMe data sets; use of segment clustering; apparent molecular lengths; preparation of two-probe geometries for NEGT-DFT calculations; NEGF-DFT results for single-linker molecules; barrier to −SMe rotation; gas-phase ionization energies; controlling Au−S binding angles through gap size; and electronic structure changes during −SMe rotation (PDF)

■ AUTHOR INFORMATION

Corresponding Author

Oliver L. A. Monti − *Department of Chemistry and Biochemistry, University of Arizona, Tucson, Arizona 85721, United States; Department of Physics, University of Arizona, Tucson, Arizona 85721, United States;* orcid.org/0000-0002-0974-7253; Phone: ++520 626 1177; Email: monti@u.arizona.edu

Authors

Nathan D. Bamberger − *Department of Chemistry and Biochemistry, University of Arizona, Tucson, Arizona 85721, United States;* orcid.org/0000-0001-5348-5695

Dylan Dyer − *Department of Chemistry and Biochemistry, University of Arizona, Tucson, Arizona 85721, United States*

Keshaba N. Parida − *Department of Chemistry and Biochemistry, University of Arizona, Tucson, Arizona 85721, United States;* orcid.org/0000-0003-3454-0868

Tarek H. El-Assaad − *Department of Chemistry and Biochemistry, University of Arizona, Tucson, Arizona 85721, United States;* orcid.org/0000-0002-7106-834X

Dawson Pursell − *Department of Chemistry and Biochemistry, University of Arizona, Tucson, Arizona 85721, United States*

Dominic V. McGrath − *Department of Chemistry and Biochemistry, University of Arizona, Tucson, Arizona 85721, United States;* orcid.org/0000-0001-9605-2224

Manuel Smeu − *Department of Physics, Binghamton University—SUNY, Binghamton, New York 13902, United States;* orcid.org/0000-0001-9548-4623

Complete contact information is available at: https://pubs.acs.org/10.1021/acs.jpcc.2c00761

Author Contributions

N.D.B., D.D., D.V.M., O.L.A.M., and M.S. conceived the research ideas. K.N.P. and T.H.E.-A. synthesized the molecules directed by D.V.M. N.D.B. and D.D. fabricated the MCBJ samples and collected the break junction data. M.S. performed the NEGF-DFT calculations and analysis. D.P. performed the gas-phase DFT calculations and analysis. N.B. wrote the manuscript with advice and input from all authors.

Notes

The authors declare no competing financial interest.

https://doi.org/10.1021/acs.jpcc.2c00761
J. Phys. Chem. C 2022, 126, 6653−6661

■ ACKNOWLEDGMENTS

Financial support from the National Science Foundation, Award No. DMR-1708443, is gratefully acknowledged. Plasma etching of MCBJ samples was performed using a plasmatherm reactive ion etcher acquired through an NSF MRI grant, Award No. ECCS-1725571. Segment clustering was performed using High Performance Computing (HPC) resources supported by the University of Arizona TRIF, UITS, and RDI and maintained by the UA Research Technologies department. Quality control was performed using a scanning electron microscope in the W. M. Keck Center for Nano-Scale Imaging in the Department of Chemistry and Biochemistry at the University of Arizona with funding from the W. M. Keck Foundation Grant. NEGF-DFT computations were performed on the Binghamton University HPC cluster, "Spiedie".

■ REFERENCES

(1) Heath, J. R. Molecular Electronics. *Annu. Rev. Mater. Res.* **2009**, *39*, 1−23.
(2) Forrest, S. R. The Path to Ubiquitous and Low-Cost Organic Electronic Appliances on Plastic. *Nature* **2004**, *428*, 911−918.
(3) Liu, Y.; Qiu, X.; Soni, S.; Chiechi, R. C. Charge Transport through Molecular Ensembles: Recent Progress in Molecular Electronics. *Chem. Phys. Rev.* **2021**, *2*, No. 021303.
(4) Ivie, J. A.; Bamberger, N. D.; Parida, K. N.; Shepard, S.; Dyer, D.; Saraiva-Souza, A.; Himmelhuber, R.; McGrath, D. V.; Smeu, M.; Monti, O. L. A. Correlated Energy-Level Alignment Effects Determine Substituent-Tuned Single-Molecule Conductance. *ACS Appl. Mater. Interfaces* **2021**, *13*, 4267−4277.
(5) Su, T. A.; Neupane, M.; Steigerwald, M. L.; Venkataraman, L.; Nuckolls, C. Chemical Principles of Single-Molecule Electronics. *Nat. Rev. Mater.* **2016**, *1*, No. 16002.
(6) Venkataraman, L.; Park, Y. S.; Whalley, A. C.; Nuckolls, C.; Hybertsen, M. S.; Steigerwald, M. L. Electronics and Chemistry: Varying Single-Molecule Junction Conductance Using Chemical Substituents. *Nano Lett.* **2007**, *7*, 502−506.
(7) Garner, M. H.; Li, H.; Chen, Y.; Su, T. A.; Shangguan, Z.; Paley, D. W.; Liu, T.; Ng, F.; Li, H.; Xiao, S.; Nuckolls, C.; Venkataraman, L.; Solomon, G. C. Comprehensive Suppression of Single-Molecule Conductance Using Destructive σ-Interference. *Nature* **2018**, *558*, 415−419.
(8) Kaliginedi, V.; Rudnev, A. V.; Moreno-García, P.; Baghernejad, M.; Huang, C.; Hong, W.; Wandlowski, T. Promising Anchoring Groups for Single-Molecule Conductance Measurements. *Phys. Chem. Chem. Phys.* **2014**, *16*, 23529−23539.
(9) Rivero, S. M.; Arroyo, P. G.; Li, L.; Gunasekaran, S.; Stuyver, T.; Mancheño, M. J.; Alonso, M.; Venkataraman, L.; Segura, J. L.; Cordón, J. C. Single-Molecule Conductance in a Unique Cross-Conjugated Tetra(Aminoaryl)-Ethene. *Chem. Commun.* **2021**, *57*, 591−594.
(10) Aradhya, S. V.; Meisner, J. S.; Krikorian, M.; Ahn, S.; Parameswaran, R.; Steigerwald, M. L.; Nuckolls, C.; Venkataraman, L. Dissecting Contact Mechanics from Quantum Interference in Single-Molecule Junctions of Stilbene Derivatives. *Nano Lett.* **2012**, *12*, 1643−1647.
(11) Widawsky, J. R.; Darancet, P.; Neaton, J. B.; Venkataraman, L. Simultaneous Determination of Conductance and Thermopower of Single Molecule Junctions. *Nano Lett.* **2012**, *12*, 354−358.
(12) Kamenetska, M.; Quek, S. Y.; Whalley, A. C.; Steigerwald, M. L.; Choi, H. J.; Louie, S. G.; Nuckolls, C.; Hybertsen, M. S.; Neaton, J. B.; Venkataraman, L. Conductance and Geometry of Pyridine-Linked Single-Molecule Junctions. *J. Am. Chem. Soc.* **2010**, *132*, 6817−6821.
(13) Meisner, J. S.; Ahn, S.; Aradhya, S. V.; Krikorian, M.; Parameswaran, R.; Steigerwald, M.; Venkataraman, L.; Nuckolls, C. Importance of Direct Metal−π Coupling in Electronic Transport Through Conjugated Single-Molecule Junctions. *J. Am. Chem. Soc.* **2012**, *134*, 20440−20445.
(14) Meng, L.; Xin, N.; Hu, C.; Wang, J.; Gui, B.; Shi, J.; Wang, C.; Shen, C.; Zhang, G.; Guo, H.; Meng, S.; Guo, X. Side-Group Chemical Gating via Reversible Optical and Electric Control in a Single Molecule Transistor. *Nat. Commun.* **2019**, *10*, No. 1450.
(15) Kim, Y. Photoswitching Molecular Junctions: Platforms and Electrical Properties. *ChemPhysChem* **2020**, *21*, 2368−2383.
(16) Martin, S.; Haiss, W.; Higgins, S. J.; Nichols, R. J. The Impact of E−Z Photo-Isomerization on Single Molecular Conductance. *Nano Lett.* **2010**, *10*, 2019−2023.
(17) Kim, Y.; Garcia-Lekue, A.; Sysoiev, D.; Frederiksen, T.; Groth, U.; Scheer, E. Charge Transport in Azobenzene-Based Single-Molecule Junctions. *Phys. Rev. Lett.* **2012**, *109*, No. 226801.
(18) Zhang, C.; Du, M.-H.; Cheng, H.-P.; Zhang, X.-G.; Roitberg, A. E.; Krause, J. L. Coherent Electron Transport through an Azobenzene Molecule: A Light-Driven Molecular Switch. *Phys. Rev. Lett.* **2004**, *92*, No. 158301.
(19) Osella, S.; Samorì, P.; Cornil, J. Photoswitching Azobenzene Derivatives in Single Molecule Junctions: A Theoretical Insight into the I/V Characteristics. *J. Phys. Chem. C* **2014**, *118*, 18721−18729.
(20) Zhang, C.; He, Y.; Cheng, H.-P.; Xue, Y.; Ratner, M. A.; Zhang, X.-G.; Krstic, P. Current-Voltage Characteristics through a Single Light-Sensitive Molecule. *Phys. Rev. B* **2006**, *73*, No. 125445.
(21) Diešková, M. Z.; Štich, I.; Bokes, P. Rigidity of the Conductance of an Anchored Dithioazobenzene Optomechanical Switch. *Phys. Rev. B* **2013**, *87*, No. 245418.
(22) Mativetsky, J. M.; Pace, G.; Elbing, M.; Rampi, M. A.; Mayor, M.; Samorì, P. Azobenzenes as Light-Controlled Molecular Electronic Switches in Nanoscale Metal−Molecule−Metal Junctions. *J. Am. Chem. Soc.* **2008**, *130*, 9192−9193.
(23) Lin, L.; Jiang, J.; Luo, Y. Elastic and Inelastic Electron Transport in Metal−Molecule(s)−Metal Junctions. *Phys. E* **2013**, *47*, 167−187.
(24) Vonlanthen, D.; Mishchenko, A.; Elbing, M.; Neuburger, M.; Wandlowski, T.; Mayor, M. Chemically Controlled Conductivity: Torsion-Angle Dependence in a Single-Molecule Biphenyldithiol Junction. *Angew. Chem., Int. Ed.* **2009**, *48*, 8886−8890.
(25) Venkataraman, L.; Klare, J. E.; Nuckolls, C.; Hybertsen, M. S.; Steigerwald, M. L. Dependence of Single-Molecule Junction Conductance on Molecular Conformation. *Nature* **2006**, *442*, 904−907.
(26) Mishchenko, A.; Zotti, L. A.; Vonlanthen, D.; Bürkle, M.; Pauly, F.; Cuevas, J. C.; Mayor, M.; Wandlowski, T. Single-Molecule Junctions Based on Nitrile-Terminated Biphenyls: A Promising New Anchoring Group. *J. Am. Chem. Soc.* **2011**, *133*, 184−187.
(27) Li, X.; Tan, Z.; Huang, X.; Bai, J.; Liu, J.; Hong, W. Experimental Investigation of Quantum Interference in Charge Transport through Molecular Architectures. *J. Mater. Chem. C* **2019**, *7*, 12790−12808.
(28) Park, Y. S.; Whalley, A. C.; Kamenetska, M.; Steigerwald, M. L.; Hybertsen, M. S.; Nuckolls, C.; Venkataraman, L. Contact Chemistry and Single-Molecule Conductance: A Comparison of Phosphines, Methyl Sulfides, and Amines. *J. Am. Chem. Soc.* **2007**, *129*, 15768−15769.
(29) Dell, E. J.; Capozzi, B.; Xia, J.; Venkataraman, L.; Campos, L. M. Molecular Length Dictates the Nature of Charge Carriers in Single-Molecule Junctions of Oxidized Oligothiophenes. *Nat. Chem.* **2015**, *7*, 209−214.
(30) Jiang, F.; Trupp, D.; Algethami, N.; Zheng, H.; He, W.; Alqorashi, A.; Zhu, C.; Tang, C.; Li, R.; Liu, J.; Sadeghi, H.; Shi, J.; Davidson, R.; Korb, M.; Naher, M.; Sobolev, A. N.; Sangtarash, S.; Low, P. J.; Hong, W.; Lambert, C. Turning the Tap: Conformational Control of Quantum Interference to Modulate Single Molecule Conductance. *Angew. Chem.* **2019**, *131*, 19163−19169.
(31) Park, Y. S.; Widawsky, J. R.; Kamenetska, M.; Steigerwald, M. L.; Hybertsen, M. S.; Nuckolls, C.; Venkataraman, L. Frustrated Rotations in Single-Molecule Junctions. *J. Am. Chem. Soc.* **2009**, *131*, 10820−10821.

https://doi.org/10.1021/acs.jpcc.2c00761
J. Phys. Chem. C 2022, 126, 6653−6661

(32) Sagan, C.; Jiang, Y.; Caban, F.; Snaider, J.; Amell, R.; Wei, S.; Florio, G. M. Oligofluorene Molecular Wires: Synthesis and Single-Molecule Conductance. *J. Phys. Chem. C* **2017**, *121*, 24945−24953.
(33) Wang, M.; Wang, Y.; Sanvito, S.; Hou, S. The Low-Bias Conducting Mechanism of Single-Molecule Junctions Constructed with Methylsulfide Linker Groups and Gold Electrodes. *J. Chem. Phys.* **2017**, *147*, No. 054702.
(34) Bamberger, N. D.; Ivie, J. A.; Parida, K.; McGrath, D. V.; Monti, O. L. A. Unsupervised Segmentation-Based Machine Learning as an Advanced Analysis Tool for Single Molecule Break Junction Data. *J. Phys. Chem. C* **2020**, *124*, 18302−18315.
(35) Bamberger, N. D.; Dyer, D.; Parida, K. N.; McGrath, D. V.; Monti, O. L. A. Grid-Based Correlation Analysis to Identify Rare Quantum Transport Behaviors. *J. Phys. Chem. C* **2021**, *125*, 18297−18307.
(36) Johnson, T. K.; Ivie, J. A.; Jaruvang, J.; Monti, O. L. A. Fast Sensitive Amplifier for Two-Probe Conductance Measurements in Single Molecule Break Junctions. *Rev. Sci. Instrum.* **2017**, *88*, No. 033904.
(37) Ohnishi, H.; Kondo, Y.; Takayanagi, K. Quantized Conductance through Individual Rows of Suspended Gold Atoms. *Nature* **1998**, *395*, 780−783.
(38) Cabosart, D.; El Abbassi, M.; Stefani, D.; Frisenda, R.; Calame, M.; van der Zant, H. S. J.; Perrin, M. L. A Reference-Free Clustering Method for the Analysis of Molecular Break-Junction Measurements. *Appl. Phys. Lett.* **2019**, *114*, No. 143102.
(39) Neese, F. The ORCA Program System. *WIREs Comput. Mol. Sci.* **2012**, *2*, 73−78.
(40) Becke, A. D. Density-functional Thermochemistry. III. The Role of Exact Exchange. *J. Chem. Phys.* **1993**, *98*, 5648−5652.
(41) Lee, C.; Yang, W.; Parr, R. G. Development of the Colle-Salvetti Correlation-Energy Formula into a Functional of the Electron Density. *Phys. Rev. B* **1988**, *37*, 785−789.
(42) Kresse, G.; Hafner, J. Ab Initio Molecular Dynamics for Liquid Metals. *Phys. Rev. B* **1993**, *47*, 558−561.
(43) Kresse, G.; Furthmüller, J. Efficient Iterative Schemes for Ab Initio Total-Energy Calculations Using a Plane-Wave Basis Set. *Phys. Rev. B* **1996**, *54*, 11169−11186.
(44) Perdew, J. P.; Burke, K.; Ernzerhof, M. Generalized Gradient Approximation Made Simple. *Phys. Rev. Lett.* **1996**, *77*, 3865−3868.
(45) Grimme, S.; Antony, J.; Ehrlich, S.; Krieg, H. A Consistent and Accurate Ab Initio Parametrization of Density Functional Dispersion Correction (DFT-D) for the 94 Elements H-Pu. *J. Chem. Phys.* **2010**, *132*, No. 154104.
(46) Taylor, J.; Guo, H.; Wang, J. Ab Initio Modeling of Quantum Transport Properties of Molecular Electronic Devices. *Phys. Rev. B* **2001**, *63*, No. 245407.
(47) Waldron, D.; Haney, P.; Larade, B.; MacDonald, A.; Guo, H. Nonlinear Spin Current and Magnetoresistance of Molecular Tunnel Junctions. *Phys. Rev. Lett.* **2006**, *96*, No. 166804.
(48) Smeu, M.; Monti, O. L. A.; McGrath, D. Phenalenyls as Tunable Excellent Molecular Conductors and Switchable Spin Filters. *Phys. Chem. Chem. Phys.* **2021**, *23*, 24106−24110.
(49) Metzger, R. M. Unimolecular Electronics. *Chem. Rev.* **2015**, *115*, 5056−5115.
(50) Martín, S.; Grace, I.; Bryce, M. R.; Wang, C.; Jitchati, R.; Batsanov, A. S.; Higgins, S. J.; Lambert, C. J.; Nichols, R. J. Identifying Diversity in Nanoscale Electrical Break Junctions. *J. Am. Chem. Soc.* **2010**, *132*, 9157−9164.
(51) Yoshida, K.; Pobelov, I. V.; Manrique, D. Z.; Pope, T.; Mészáros, G.; Gulcur, M.; Bryce, M. R.; Lambert, C. J.; Wandlowski, T. Correlation of Breaking Forces, Conductances and Geometries of Molecular Junctions. *Sci. Rep.* **2015**, *5*, No. 9002.
(52) Wu, S.; González, M. T.; Huber, R.; Grunder, S.; Mayor, M.; Schönenberger, C.; Calame, M. Molecular Junctions Based on Aromatic Coupling. *Nat. Nanotechnol.* **2008**, *3*, 569−574.
(53) Li, H.; Garner, M. H.; Shangguan, Z.; Zheng, Q.; Su, T. A.; Neupane, M.; Li, P.; Velian, A.; Steigerwald, M. L.; Xiao, S.; Nuckolls, C.; Solomon, G. C.; Venkataraman, L. Conformations of Cyclopentasilane Stereoisomers Control Molecular Junction Conductance. *Chem. Sci.* **2016**, *7*, 5657−5662.
(54) Batra, A.; Darancet, P.; Chen, Q.; Meisner, J. S.; Widawsky, J. R.; Neaton, J. B.; Nuckolls, C.; Venkataraman, L. Tuning Rectification in Single-Molecular Diodes. *Nano Lett.* **2013**, *13*, 6233−6237.
(55) Verzijl, C. J. O.; Gil, J. A. C.; Perrin, M. L.; Dulić, D.; van der Zant, H. S. J.; Thijssen, J. M. Image Effects in Transport at Metal-Molecule Interfaces. *J. Chem. Phys.* **2015**, *143*, No. 174106.
(56) Toher, C.; Filippetti, A.; Sanvito, S.; Burke, K. Self-Interaction Errors in Density-Functional Calculations of Electronic Transport. *Phys. Rev. Lett.* **2005**, *95*, No. 146402.
(57) Sangtarash, S.; Huang, C.; Sadeghi, H.; Sorohhov, G.; Hauser, J.; Wandlowski, T.; Hong, W.; Decurtins, S.; Liu, S.-X.; Lambert, C. J. Searching the Hearts of Graphene-like Molecules for Simplicity, Sensitivity, and Logic. *J. Am. Chem. Soc.* **2015**, *137*, 11425−11431.

https://doi.org/10.1021/acs.jpcc.2c00761
J. Phys. Chem. C 2022, 126, 6653−6661